JOURNAL OF Materials CHEMISTRY

Conducting redox polymers: investigations of polythiophene–Ru(bpy)$_3^{n+}$ hybrid materials

S. Sherry Zhu, Richard P. Kingsborough and Timothy M. Swager*

Department of Chemistry and Center for Materials Science and Engineering, Massachusetts Institute of Technology, Cambridge, MA 02139, USA

Received 21st April 1999, Accepted 14th June 1999

A series of thiophene-appended Ru^{II}(bpy)$_3$ derivatives, Ru(**1**)$_3$, Ru(**2**)$_3$, Ru(**3**)$_3$, Ru(bpy)$_2$(**1**), and Ru(bpy)$_2$(**2**), and their resulting polymers have been synthesized and characterized. The bpy ligands 5,5′-bis(5-(2,2′-bithienyl))-2,2′-bipyridine, **1**, 4,4′-bis(5-(2,2′-bithienyl))-2,2′-bipyridine, **2**, and 4-(5-(2,2′-bithienyl))-2,2′-bipyridine, **3**, all contain electrochemically polymerizable bithienyl moieties. The monomers Ru(**2**)$_3$, Ru(**3**)$_3$, Ru(bpy)$_2$(**1**) and Ru(bpy)$_2$(**2**) display spectroscopic features that are similar to the ligand-based and MLCT bands found for Ru(bpy)$_3$. The cyclic voltammograms of all of these polymers display both metal-centered and thiophene-based electroactivity. High redox conductivity was found in poly(Ru(**2**)$_3$) and poly(Ru(**3**)$_3$) for both the thiophene-based oxidation and metal-based reduction processes. These results indicate that the polymers display charge localization for both the metal complexes as well as the tetrathienyl connecting units. The degree of interconnection (number of linkages) as well as the substitution pattern were found to control the conductivity of these polymers. The highest conductivity (3.3×10^{-3} S cm^{-1}) was found for poly(Ru(**2**)$_3$), which is able to have up to 6 linkages with other ruthenium complexes as well as possessing a 4,4′-substitution pattern that allows effective orbital overlap of the conjugated polymer backbone with the ruthenium centers.

Introduction

Conjugated organic polymers incorporating redox-active transition metal centers that are coupled to the π system offer the potential to enhance the rate and range of electron transfer between localized metal-centered redox sites relative to non-conjugated polymeric systems.[1–6] Integration of transition metal complexes into a conducting polymer framework also presents opportunities for unique photophysical, photochemical, and electrochemical properties, catalysis, as well as the ability to create sensors for small molecules (O_2, CO, NO) or anions (Cl^-, PO_4^{2-}).[7–15] Numerous investigations have focused on nonconjugated polymers containing isolated Ru(bpy)$_n$L$_{3-n}$,[8–15] ferrocene,[16] and other redox-active metal centers.[6,17] In these systems the charge hopping between these isolated metal centers can result in redox conductivity. There are far fewer investigations of polymers wherein redox-active metal centers are in electronic communication through conjugated bridges.[1–6,8,18] These limited studies nevertheless suggest that this is a promising approach to an important class of materials.

We have recently communicated the synthesis of a polythiophene–Ru(bpy)$_3^{2+}$ hybrid material,[1] poly(Ru(**1**)$_3$), by the anodic polymerization of a tris[5,5′-bis(5-(2,2′-bithienyl))-2,2′-bipyridine]ruthenium(II) complex, Ru(**1**)$_3$ (Chart 1). The bithiophene groups were substituted at the 5,5′-positions of bipyridine to produce a monomeric bipyridine unit (**1**) in which there is extended conjugation across the bipyridine. In the case of poly(Ru(**1**)$_3$) the ruthenium centers are coordinated directly to the conjugated polymer backbone, allowing for interactions between the polymer and the metal centers. However, the 5,5′-substitution of the bipyridine of poly(Ru(**1**)$_3$) produces limited interactions between neighboring metal centers as a result of the non-conjugated *meta* relationship between the thiophenes and the metal binding sites, generating a system where the ruthenium complexes and the polymer backbone have isolated electrochemical activities. In spite of this localization, we found this hybrid system to exhibit a redox conductivity of 9.4×10^{-4} S cm^{-1} involving self-exchange between localized Ru(**1**)$_3^{n+}$ sites,[1] which is high relative to other redox conductors. The metal-free polymer, poly(**1**), displayed conductivity derived from charge delocalization in both n-doped and p-doped states.[1]

Changing the position of the bithiophene moieties to the 4- and 4′-positions on the bipyridine ligand creates a system in which the d_{xz} and d_{yz} orbitals of the ruthenium center can communicate with neighboring metal centers by overlapping with the π orbitals of the conjugated bridge. This is possible due to the *para* relationship between the ruthenium centers and the tetrathienyl bridge, allowing for the maximum electronic communication between the metal complexes. In this paper we describe the polymerization of two new homoleptic complexes, Ru(**2**)$_3$ and Ru(**3**)$_3$, which have bithiophene groups at the 4,4′- and 4-position of the bipyridine ligand, respectively, as well as the heteroleptic complexes Ru(bpy)$_2$(**1**) and Ru(bpy)$_2$(**2**), which form polymers having Ru(bpy)$_2$ complexes appended to an organic backbone. The metal-free polymer poly(**2**) has also been prepared by oxidative polymerization. Owing to the *meta* relationship of the bithiophene moieties in this polymer and a lack of extended conjugation, no drain current (conductivity) was detected under our experimental conditions. The hybrid polymers, poly(Ru(**2**)$_3$), poly(Ru(**3**)$_3$), poly(Ru(**1**)(bpy)$_2$) and poly(Ru(**2**)(bpy)$_2$), display metal-centered redox-type conductivity that is comparable to the conductivity observed from the tetrathienyl (organic) portion of the polymer. For comparison, additional optical absorption and electrochemical studies of poly(Ru(**1**)$_3$) are also reported.

Results and discussion

Synthesis and characterization of Ru(bpy)$_3$ derivatives

We previously reported the synthesis of 5,5′-bis(5-(2,2′-bithienyl))-2,2′-bipyridine **1** from 5,5′-dibromo-2,2′-bipyridine[19] *via* standard Stille coupling methods (Scheme 1).[1] 4,4′-Bis(5-(2,2′-bithienyl))-2,2′-bipyridine **2** was prepared by similar methods from 4,4′-dibromo-2,2′-bipyidine.[20] Mononitration of 2,2′-bipyridine-*N*,*N*′-dioxide[21] with KNO_3 in 98% H_2SO_4 afforded a route to 4-bromo-2,2′-bipyridine (Scheme 2), which can be converted into 4-(5-(2,2′-bithienyl))-2,2′-bipyridine **3** as above

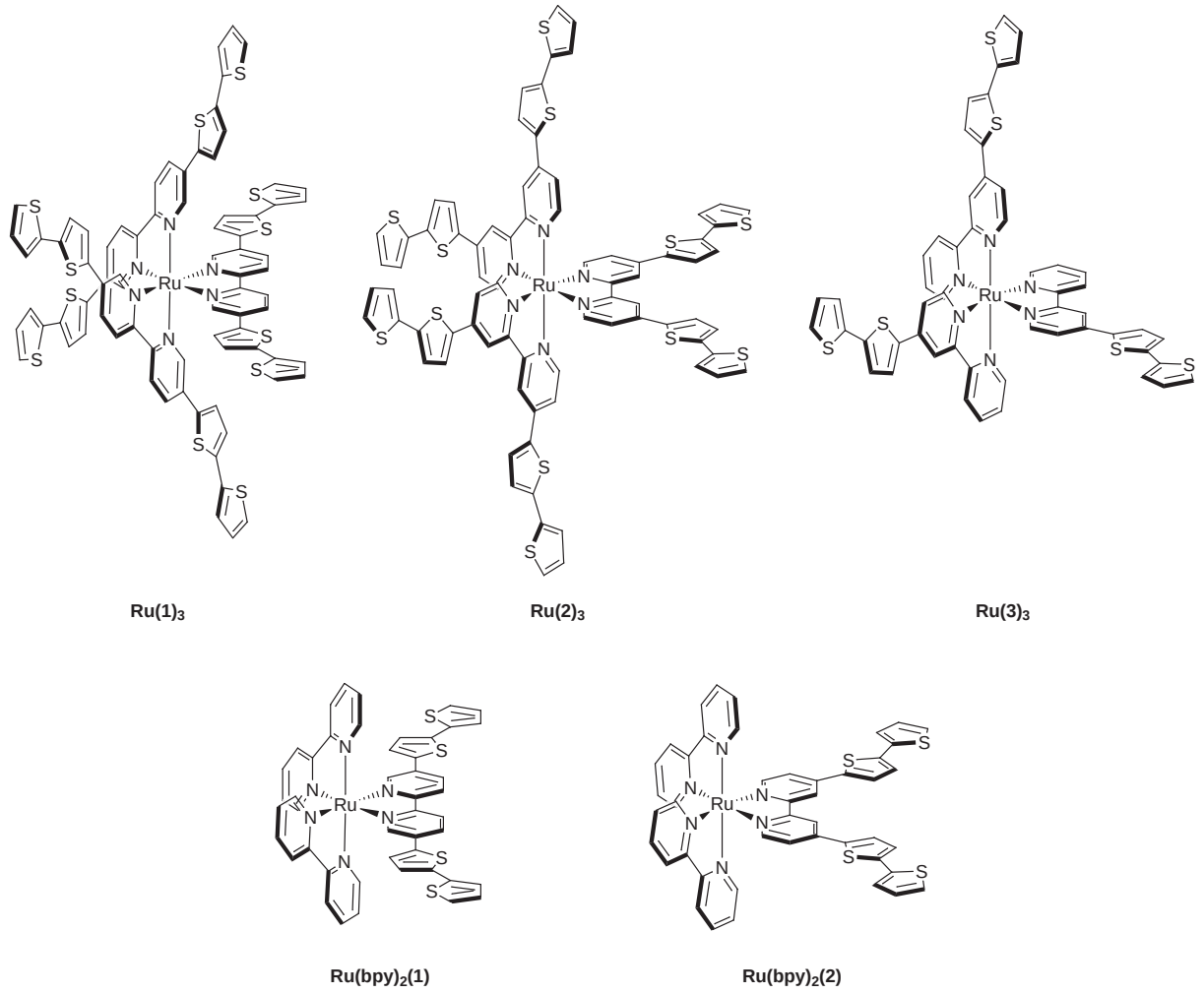

Chart 1

(Scheme 1). These compounds are characterized as low solubility yellow solids which show satisfactory ^{1}H NMR, mass spectroscopy, and elemental analysis.

The homoleptic ruthenium complexes Ru(**1**)$_3$,[1] Ru(**2**)$_3$, and Ru(**3**)$_3$ were synthesized by standard procedures.[22] The ^{1}H NMR spectra of Ru(**1**)$_3$[1] and Ru(**2**)$_3$ display only one set of ligand-based proton signals, indicative of the expected D_3 symmetry of the octahedral metal centers. Complex Ru(**3**)$_3$ also exhibits one set of ligand-based proton signals that are broadened due to the multiple isomers that are present. The heteroleptic complexes Ru(**1**)(bpy)$_2$ and Ru(**2**)(bpy)$_2$ were prepared in similar fashion from *cis*-RuCl$_2$(bpy)$_2$ and the appropriate bipyridyl ligand and show ^{1}H NMR spectra which are consistent with a C_2 symmetry imposed by an ML_2L' ligand set in a six coordinate complex.

The UV–vis absorption spectra of the three ligands and their ruthenium complexes are shown in Fig. 1. The spectrum of **1** displays the lowest energy ligand-based absorption of the series at $\lambda_{max} = 396$ nm, due to the extended conjugation afforded by the 5,5′-bithienyl moieties. The bithienyl substituents on the bipyridine result in a substantially higher λ_{max} as compared to parent bipyridine ($\lambda_{max} = 283$ nm). Bipyridine **2** exhibits a slightly higher energy absorption maximum at 361 nm due to its shorter conjugation length than bipyridine **1**. Removal of one bithienyl moiety in bipyridine **3** results in a further blue shift of the absorption at $\lambda_{max} = 354$ nm (Fig. 1).

The UV–vis spectra of the ruthenium complexes show much larger absorption cross-sections than those of the parent ligands (Fig. 1). Similar absorption coefficient enhancements of ruthenium complexes over 'free' ligands have also been found by others in diphenyl substituted Ru(bpy)$_3$ complexes.[23] The spectra are dominated by both ligand-based and metal-to-ligand charge transfer (MLCT) absorptions. The complex Ru(**1**)$_3$ displays a broad absorption peak at 454 nm accompanied by a slight shoulder at 410 nm. The broad absorption is most likely a combination of ligand-centered and MLCT bands and is almost coincident with that of Ru(bpy)$_3$. In the case of Ru(**2**)$_3$ the absorption at 404 nm is likely a ligand-based transition which is red shifted from the 'free' ligand absorption due to coordination. These shifts are expected based on the donor–acceptor nature of the ligand chromophore. The strong absorption centered at 507 nm (Table 1 and Fig. 1), which is far removed from the optical spectra of free **2**, is MLCT in nature. These spectral features, while similar to those of Ru(bpy)$_3$(PF$_6$)$_2$,[24] have both ligand-based and MLCT absorbances that are red shifted due to the electron-rich bithienyl moieties. Complex Ru(**3**)$_3$ also displays a similar optical absorption spectrum, although the red shift is not as substantial as in Ru(**2**)$_3$. The latter is likely due to the diminished number of electron donating groups on the bipyridine ligands.

The heteroleptic complexes display features similar to their homoleptic counterparts. Complex Ru(**1**)(bpy)$_2$ displays a UV–vis spectrum that is intermediate between those of Ru(bpy)$_3$ and Ru(**1**)$_3$. Two intense waves at 289 and 455 nm can be attributed to absorption by the bpy ligand and a MLCT absorption, respectively. The intense MLCT band of Ru(bpy)$_2$(**1**) is nearly coincident with that of Ru(**1**)$_3$, signifying that the *meta* relationship between the bithienyl moieties and the ruthenium center exerts little influence on the MLCT

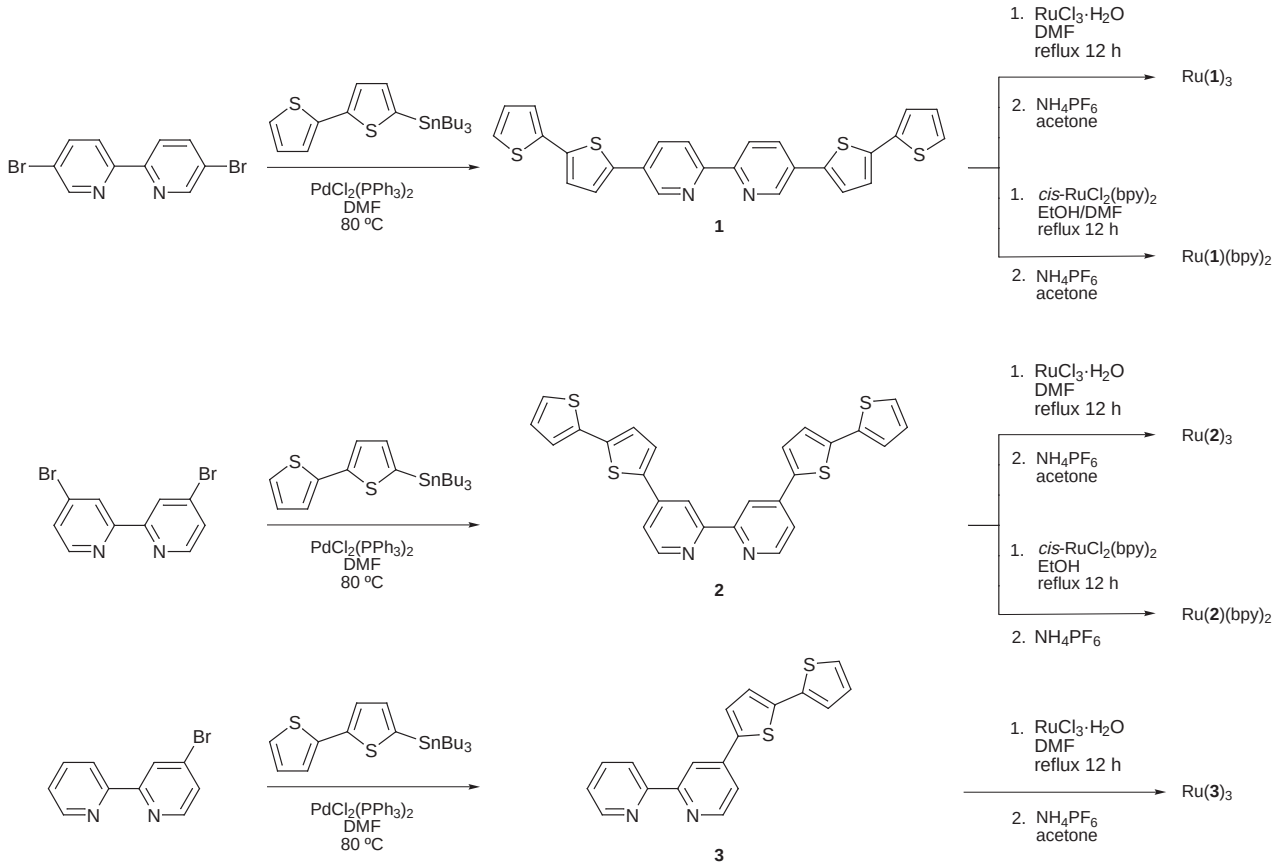

Scheme 1

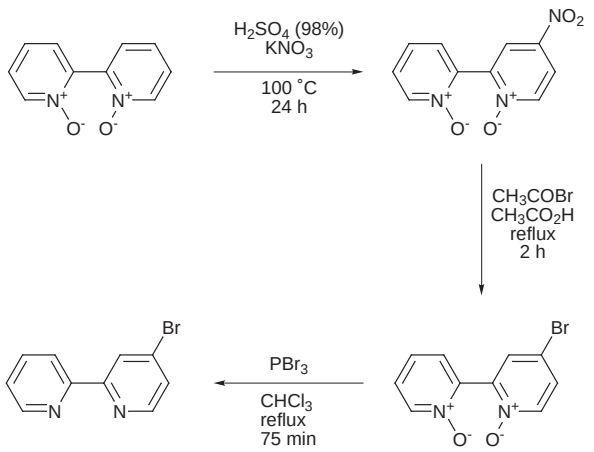

Scheme 2

absorption band. Complex $Ru(bpy)_2(\mathbf{2})$ shows an intense ligand-based absorbance with a λ_{max} at 291 nm (Fig. 1). It also possesses two resolved, strong absorptions at 392 and 409 nm, as well as two MLCT bands at 465 and 485 nm. The lower absorptivity of the 392 and 409 nm bands relative to those of $Ru(\mathbf{2})_3$ supports their assignment as ligand-centered transitions. Multiple MLCT bands have been observed for other mixed-chelate complexes in which there are separate transitions for each ligand.

Electrochemical studies

The electrochemical behavior of all the reported complexes has been investigated and found to depend on the amount and position of the bithienyl substitution on the bipyridine ligand. The reductive processes in ruthenium polypyridyl complexes correlate with the reduction potential of the 'uncoordinated' ligands.[25–29] In this case we are able to observe the *meta* and *para* effects of bithienyl substitution as well as the overall number of bithienyl moieties that can perturb the electronic structure of the complex.

The reduction potentials (referenced to the $Fc–Fc^+$ couple) in CH_2Cl_2 solutions for the ruthenium complexes studied here are presented in Table 1. Data taken in MeCN solution for selected complexes are also presented for comparison to published $[Ru(bpy)_3][PF_6]_2$ electrochemistry, as well as our previous studies[1] of $Ru(\mathbf{1})_3$. One trend that is immediately obvious is that substitution of bithienyl residues onto the bipyridine ligand results in reduction at more positive potentials than the parent $[Ru(bpy)_3][PF_6]_2$. For the homoleptic series, only two reversible redox waves are observed, not the three that are seen in $[Ru(bpy)_3][PF_6]_2$.[30] Continued sweeping to more negative potentials resulted in decomposition. Complex $Ru(\mathbf{1})_3$ shows an approximately 250 mV more positive reduction potential in CH_2Cl_2 than $[Ru(bpy)_3][PF_6]_2$. Changing the position of the bithienyl units to the 4- and 4′-positions in $Ru(\mathbf{2})_3$ resulted in a reduction potential 70–80 mV more negative than $Ru(\mathbf{1})_3$. Complex $Ru(\mathbf{3})_3$, with only one bithienyl group attached to the bipyridine ligand, affords only a moderate positive shift (80–120 mV) in the reduction potentials relative to $[Ru(bpy)_3][PF_6]_2$. Consistent with the fact that the reduction processes of these complexes are principally ligand-centered, their relative reduction potentials appear to be related to the delocalization in the ligand. Apparently the more highly conjugated ligand, **1**, is more stable in its reduced state.

The heteroleptic monomers also show shifts in the reduction potentials. In CH_2Cl_2 solution $Ru(bpy)_2(\mathbf{1})$ shows only one reduction wave at -1.50 V, unlike the homoleptic $Ru(\mathbf{1})_3$; $Ru(bpy)_2(\mathbf{2})$ also displays only one redox wave at -1.73 V. However, in MeCN solution different electrochemistry is observed. Complex $Ru(bpy)_2(\mathbf{1})$, like $[Ru(bpy)_3][PF_6]_2$, displays three one-electron redox waves at -1.49, -1.84 and

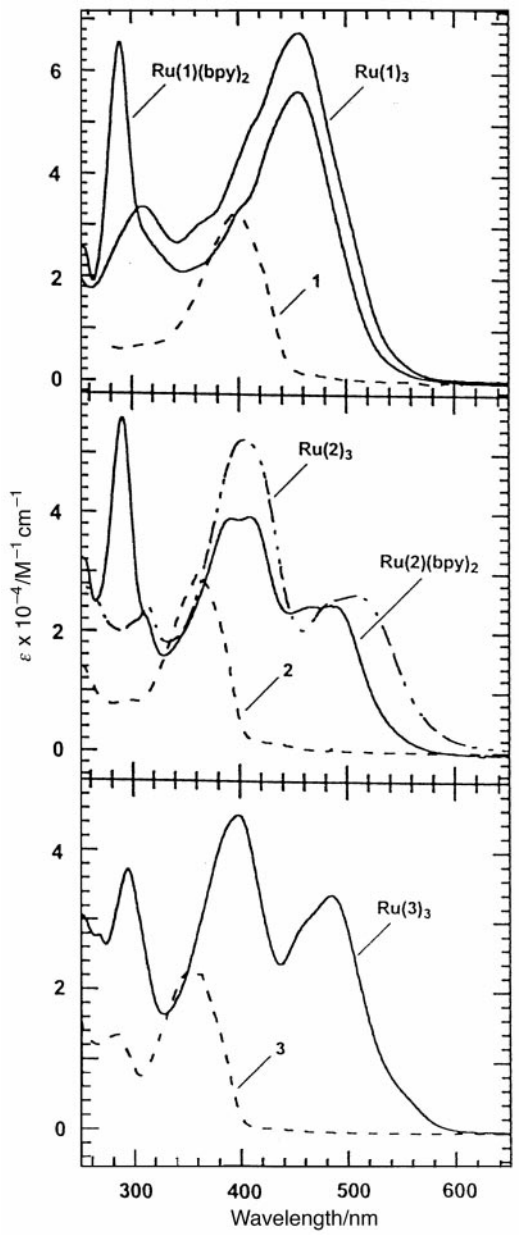

Fig. 1 The UV–vis spectra of ligands **1**, **2** and **3** and the ruthenium complexes Ru(**1**)$_3$, Ru(**2**)$_3$, Ru(**3**)$_3$, Ru(bpy)$_2$(**1**) and Ru(bpy)$_2$(**2**) in CH_2Cl_2.

−2.03 V. Complex Ru(bpy)$_2$(**2**) displays two one-electron redox waves at −1.60 and −1.86 V, which are very similar to those observed for Ru(**3**)$_3$. The reason for the solvent dependency is unclear. The similarity of the redox potentials of Ru(**3**)$_3$ and Ru(bpy)$_2$(**2**) suggests that only a single bithienyl-substituted ligand need be present to affect the first reduction. This is also observed in the UV–vis spectra, as these two complexes display bands at very similar wavelengths.

Polymeric films of the ruthenium complexes were deposited onto interdigitated microelectrodes[31] by the anodic polymerization of CH_2Cl_2 monomer solutions. Once synthesized, the films were rinsed and transferred to a cell containing fresh 0.1 M Bu_4NPF_6–CH_2Cl_2 for electrochemical analysis and redox conductivity measurements. The polymer films were electrochemically deposited on 5 μm interdigitated microelectrodes such that the film served as the connection between the two sets of independently addressable electrodes. After a small potential difference (V_D) was applied between the two electrodes, the potentials of both electrodes were scanned *versus* the reference electrode at a slow rate. The drain current (i_D) that flowed between the two sets of electrodes, source and drain, can then be observed as a function of the applied potential. This drain current can be related directly to absolute conductivity (σ) by eqn. (1), where W is the distance between the electrodes (5 μm), n the number of spaces between electrodes, T the thickness of the film in the region between the electrodes, and L the length of the finger.

$$\sigma = \frac{i_D}{V_D} \cdot \frac{W}{nTL} \quad (1)$$

The thickness was determined for a film of poly(Ru(**1**)$_3$) and from this value and the surface coverage Γ calculated from integrating the ruthenium waves a ruthenium site concentration of 3.8×10^{-4} mol cm^{-3} was determined. This value is similar to that observed for other polymeric systems.† In the polymers investigated here, where $T \ll W$ (the calculated T was between 8.0×10^{-6} and 3.0×10^{-5} cm), the calculated conductivity presented here represents a lower limit due to the thin nature of the polymer film. Specifically, not all of the polymer measured will be in the gap between the electrodes and the thickness at the center of the gap is expected to be less than T.

In our previous communication[1] we described the electrochemical properties of poly(**1**) and poly(Ru(**1**)$_3$) in MeCN solutions. Poly(**1**) displayed conductivity in both the oxidative and reductive regions. Poly(Ru(**1**)$_3$) showed electrochemical processes typical of materials composed of thienyl moieties and ruthenium complexes. There was little difference in the thienyl electrochemistry upon coordination of the ruthenium centers; however, new Ru(bpy)$_3$-centered reduction processes could be observed in the reduction region. Owing to the limited stability of this polymer in the more nucleophilic MeCN solvent, we reexamined the poly(Ru(**1**)$_3$) electrochemistry in CH_2Cl_2. Examination of the polymer CV (Fig. 2a) shows that the charge passed by the ruthenium bipyridyl-

Table 1 Electrochemical and electronic absorption characteristics of monomers and polymers investigated[a]

Complex	$E_{1/2}$/V *vs.* Fc–Fc$^+$	λ_{max}[b]/nm
[Ru(bpy)$_3$][PF$_6$]$_2$	−1.74[c] −1.93[c]	290, 452
[Ru(**1**)$_3$][PF$_6$]$_2$	−1.48 (−1.48)[c] −1.68 (−1.68)[c]	310, 400, 454
[Ru(**2**)$_3$][PF$_6$]$_2$	−1.56 −1.75	404, 507
[Ru(**3**)$_3$][PF$_6$]$_2$	−1.62 −1.85	398, 486
[Ru(bpy)$_2$(**1**)][PF$_6$]$_2$	−1.50 (−1.49)[c] (−1.84)[c] (−2.03)[c]	289, 399, 455
[Ru(bpy)$_2$(**2**)][PF$_6$]$_2$	−1.73[d] (−1.60)[c] (−1.86)[c]	392, 409, 465, 485
poly(Ru(**1**)$_3$)	−1.40 −1.59	412, 470
poly(Ru(**2**)$_3$)	−1.60 −1.76	408, 506
poly(Ru(**3**)$_3$)	−1.67 −1.79	—
poly(Ru(bpy)$_2$(**1**))	−1.49	500
poly(Ru(bpy)$_2$(**2**))	−1.92	518
poly(**1**)	−2.02	480
poly(**2**)	−2.07	—

[a]Unless noted otherwise, electrochemical measurements were performed in 0.1 M Bu_4NPF_6–CH_2Cl_2 solution at a platinum button electrode at a scan rate of 50 mV s^{-1}. [b]In CH_2Cl_2 solution. [c]In 0.1 M Bu_4NPF_6–MeCN solution at a platinum button electrode at a scan rate of 100 mV s^{-1}. [d]Only one redox process observed.

†The same value was used for all of the compounds; however, these complexes all have slightly different volumes due to their shapes and density of polymerizable appendages. We previously determined the redox conductivity of poly(Ru(**1**)$_3$) in MeCN as 9.4×10^{-4} S cm^{-1} by measuring the thickness of the polymers by SEM.

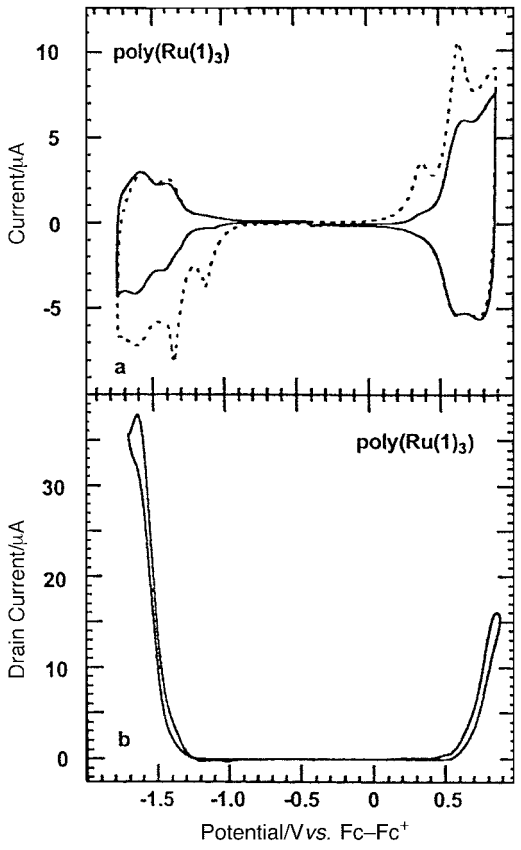

Fig. 2 (a) Cyclic voltammograms of poly($Ru(\mathbf{1})_3$) in 0.1 M Bu_4NPF_6–CH_2Cl_2 on 5 μm interdigitated microelectrodes at a sweep rate of 50 mV s^{-1}. The dotted lines indicate the first scan in each direction from −0.4 V and the solid lines show the third scan. (b) Drain current profile of poly($Ru(\mathbf{1})_3$) on the same electrode at a sweep rate of 3 mV s^{-1} with an offset potential of 40 mV.

based reduction process is approximately 1.9 times smaller than that passed due to the tetrathienyl oxidation.

For a poly$(Ru(L)_x(bpy)_{3-x})^{2+}$ complex three distinct electrochemical processes are expected: (1) the oxidation of the tetrathienyl groups, (2) the $Ru^{2+/3+}$ couple, and (3) a primarily ligand-based reduction of the metal bipyridyl groups. Previous investigations[2] in our laboratory have established that poly(**1**) and its metal complexes undergo two sequential one-electron tetrathienyl-based oxidation processes. The first occurs below the expected potential of the $Ru^{2+/3+}$ redox couple. However, while the second anodic wave may obscure a $Ru^{2+/3+}$ process, in some cases we believe that positive charge from the oxidized tetrathienyl groups shifts the $Ru^{2+/3+}$ wave to higher potentials than would be predicted from the optical band gaps. The electrochemical behavior of poly($Ru(\mathbf{1})_3$) is very similar to that of complexes of **1** with non-redox active metals and hence we believe that the $Ru^{2+/3+}$ couple is shifted to higher potential as a result of the combined electrostatic and inductive effects from the oxidized ligands. Our understanding of the nature of the electrochemistry also provides a means to evaluate the degree of polymerization of the thienyl groups. Considering that only ligand-based electrochemistry occurs below the decomposition potential for poly($Ru(\mathbf{1})_3$), we expected that, if all of the bithienyl moieties underwent oxidative coupling, a 3:1 coulombic ratio of the thienyl-based wave to the $Ru(bpy)_3$-based waves would be observed. Non-polymerized bithienyl groups oxidize at a higher potential, hence this ratio provides a measure of the tetrathiophene-to-Ru ratio. Based on this figure, we calculate that each ruthenium complex is, on average, connected to two neighbors.

Also observed in the poly($Ru(\mathbf{1})_3$) CV is an electrochemically irreversible charge trapping wave during the first reductive sweep (Fig. 2a, dotted line). Scanning the oxidative and reductive regions separately (solid line) results in no charge trapping peaks. Similar charge trapping phenomena have been observed in other thienyl- or $Ru(bpy)_3$-based polymers.[32] While different explanations for charge trapping have been reported,[32] we believe it is likely due to a structural change in the polymers during the reduction process.

The conductivity profile in CH_2Cl_2 also displays two conductivity maxima (Fig. 2b) associated with the oxidized tetrathienyl linker and the reduced $Ru(bpy)_3$ centers, with the maximum conductivity (1.2×10^{-3} S cm^{-1}) associated with the $Ru(bpy)_3$ complexes. This value is an order of magnitude higher than the conductivity of a highly conductive non-conjugated polymer. For example, poly$(Os(bpy)_2(4\text{-vpy})_2)$ (4-vpy = 4-vinylpyridine) was shown by Chidsey and Murray to have a conductivity of 1.2×10^{-4} S cm^{-1}.[12e]

Bipyridine **2**, with the pseudo-*meta* relationship between the bithienyl units, is expected to have limited conjugation. Nevertheless, CH_2Cl_2 solutions of **2** can be oxidatively polymerized to generate red films of poly(**2**). The CV of poly(**2**) is shown in Fig. 3a and is characterized by a broad, unresolved tetrathienyl oxidative process centered at 0.68 V. Similar to poly(**1**),[1] poly(**2**) also exhibits a stable reduction wave centered at −2.13 V. Charge trapping processes are also observed when sweeping the entire oxidative and reductive regions. As expected for these polymers with no extended conjugation due to the *meta* linkage, no detectable conductivity (our detection limit is 10^{-6}–10^{-7} S cm^{-1}) was observed under our experimental conditions.

Films of poly$(Ru(\mathbf{2})_3)$ exhibit cyclic voltammograms that are very different to that of poly(**2**). They are characterized by two well defined tetrathienyl-based redox waves at 0.57 and 0.85 V (Fig. 3b) as well as two $Ru(bpy)_3$-based redox waves at −1.60 and −1.76 V. Again we believe the charged thienyl groups shift the $Ru^{2+/3+}$ redox couple to more positive potentials. These two $Ru(bpy)_3$-based reduction processes occur in a region where poly(**2**) is inactive. The reduction potentials of poly$(Ru(\mathbf{2})_3)$ are more negative than those of poly$(Ru(\mathbf{1})_3)$, which follows the trend observed in the monomeric complexes. However, in contrast to poly$(Ru(\mathbf{1})_3)$, the reduction potentials of poly$(Ru(\mathbf{2})_3)$ are now more negative than those of its monomer. Continuous sweeping of the reduction region results in a slow decline in the current of the reduction waves, indicating slow decomposition of the polymer. The coulombic ratio of these two processes (Q_{ox} : Q_{red}) was found to be 2.3 : 1, indicating an average of 4.6 dithienyl groups underwent oxidative coupling during the anodic polymerization.

The conductivity profile of poly$(Ru(\mathbf{2})_3)$ on interdigitated microelectrodes is shown in Fig. 3c. It was found that while the $Ru(bpy)_3$-centered reduction process was less stable than the tetrathienyl-based oxidation, both of these regions display similar conducitivity. As expected for redox conduction, the conductivity profile displays a maximum at −1.76 V with a small shoulder at −1.60 V, which are coincident with the potentials of the two reduction processes observed in CV. Poly$(Ru(\mathbf{2})_3)$ exhibits a slightly higher conducting current when oxidized, with the conductivity reaching a maximum at 0.85 V accompanied by a shoulder at 0.58 V. The correlation between the redox potentials of the tetrathienyl waves and the conductivity suggests that the anodic conductivity also results from hopping between charges localized on the thienyl moieties. The conductivity maximum of poly$(Ru(\mathbf{2})_3)$ observed for the $Ru(bpy)_3$-based processes is 3.3×10^{-3} S cm^{-1}, which is 2.7 times greater than that observed for poly$(Ru(\mathbf{1})_3)$. This indicates that the self exchange conductivity between adjacent ruthenium complexes is further enhanced by having the ruthenium bipyridyl complexes connected by a tetrathienyl bridge in the *para* position. It is important to emphasize that the Ru^{2+} metal center facilitates conduction resulting from the oxidized tetrathienyl units relative to poly(**2**), which had a

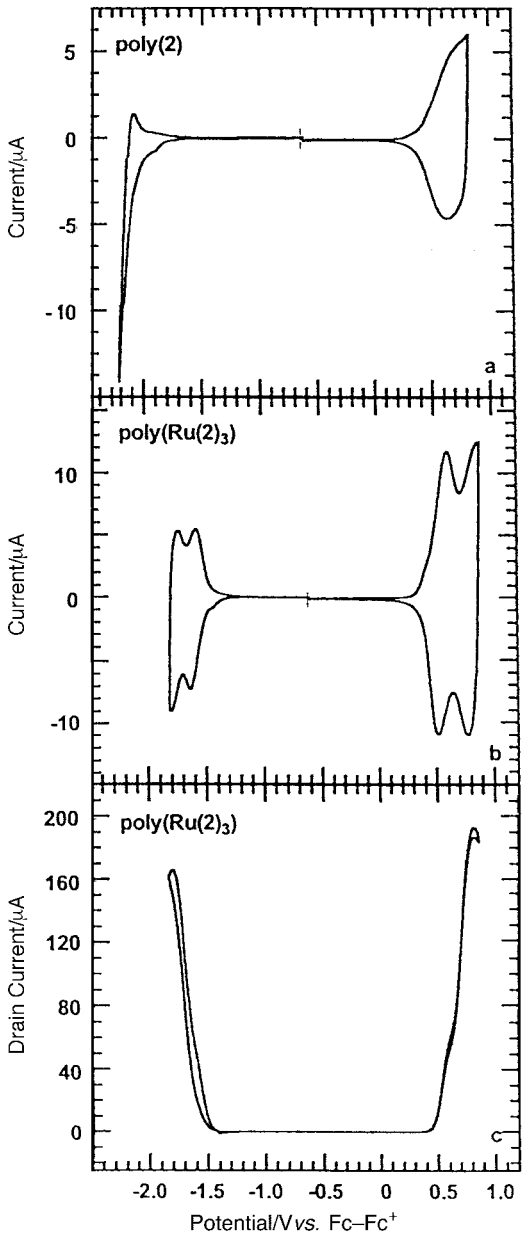

Fig. 3 (a) Cyclic voltammograms of poly(**2**) in 0.1 M Bu_4NPF_6–CH_2Cl_2 on 5 μm interdigitated microelectrodes at a sweep rate of 50 mV s^{-1} in each direction from −0.6 V. (b) Cyclic voltammograms of poly($Ru(\mathbf{2})_3$). Conditions as in (a). (c) Drain current profile of poly($Ru(\mathbf{2})_3$) on the same electrode at a sweep rate of 5 mV s^{-1} with an offset potential of 40 mV.

much lower ($<10^{-6}$ S cm^{-1}) conductivity value. In effect, the *para* relationship between the Ru^{2+} and the tetrathienyl groups creates a conjugation path. An additional factor that may contribute is that ruthenium complexation exerts changes in the orbital energies which facilitate conductivity. Other features which have not fully been investigated at present include the effects of chain–chain interactions to result in enhanced interchain conduction.

Complex $Ru(\mathbf{3})_3$ was designed to have only one bithienyl substituent per bipyridine ligand. Keeping this in mind, the electrochemistry of poly($Ru(\mathbf{3})_3$) is very similar to that of poly($Ru(\mathbf{2})_3$) (Fig. 4a). Two $Ru(bpy)_3$-based reduction waves were observed at −1.67 and −1.79 V; however, the peak current of these waves decreased with repeated sweeping. The potentials of the reduction waves are more negative than those of poly($Ru(\mathbf{2})_3$), consistent with comparisons of the monomeric species. In the tetrathienyl oxidation region two well defined waves are observed at 0.55 and 0.84 V. The coulombic ratio

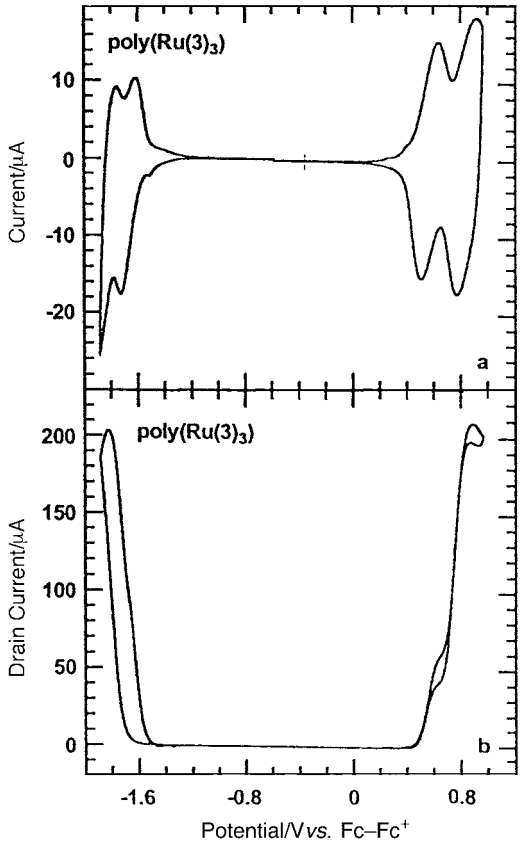

Fig. 4 (a) Cyclic voltammograms of poly($Ru(\mathbf{3})_3$) in 0.1 M Bu_4NPF_6–CH_2Cl_2 on 5 μm interdigitated microelectrodes at a sweep rate of 50 mV s^{-1} in each direction from −0.6 V. (b) Drain current profile of poly($Ru(\mathbf{3})_3$) on the same electrode at a sweep rate of 5 mV s^{-1} with an offset potential of 40 mV.

of these signals was found to be 1.26:1, close to the ideal 1.5:1, indicative of an average coupling of 2.5 bithienyl units per monomer during electrochemical polymerization. The higher polymerization ratio observed for poly($Ru(\mathbf{3})_3$) may be due to the less crowded nature of $Ru(\mathbf{3})_3$, allowing for higher crosslinking. In spite of the reduced stability of poly($Ru(\mathbf{3})_3$) to reduction, conductivity measurements were successfully performed (Fig. 4b). Like the other homoleptic polymers, poly($Ru(\mathbf{3})_3$) shows redox conductivity in both the oxidative and reductive regions. We have determined the conductivity due to self-exchange between the ruthenium complexes to be 1.73×10^{-3} S cm^{-1}. The intermediate conductivity value between poly($Ru(\mathbf{1})_3$) and poly($Ru(\mathbf{2})_3$) suggests that, while the redox conductivity is enhanced by having the tetrathienyl bridges *para* to the ruthenium, a higher number of linkages seems to facilitate a higher self-exchange between neighboring ruthenium complexes.

We also investigated structures wherein $Ru(bpy)_2$ complexes are tethered to poly(**1**) or poly(**2**) backbones. The cyclic voltammogram of poly($Ru(bpy)_2(\mathbf{1})$) is shown in Fig. 5a. There are a number of significant differences in comparison to poly($Ru(\mathbf{1})_3$). In the reductive region, unlike poly($Ru(\mathbf{1})_3$), only one reduction process is observed, which is coincident with monomer reduction. In the oxidative region there are two waves of unequal charge. In comparing the first tetrathienyl-based redox wave to the ruthenium reduction wave, the second oxidation wave does not appear to be a one-electron process. The larger nature of the second oxidation wave suggests that a $Ru^{2+/3+}$ couple may be present in addition to a second one-electron oxidation of the tetrathienyl group. This is also consistent with a smaller electrostatic and inductive perturbation caused by having only one oxidizable ligand attached to the Ru^{2+} center. The coulombic ratio of the oxidation to

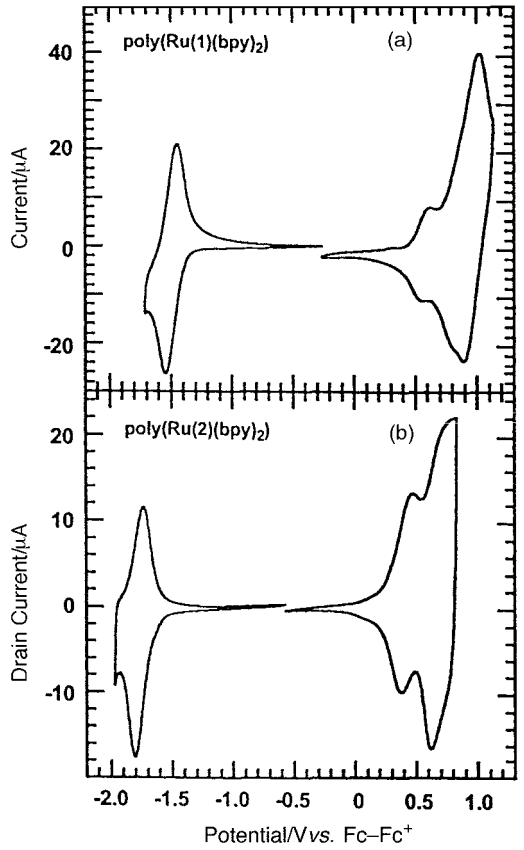

Fig. 5 (a) Cyclic voltammograms of poly($Ru(bpy)_2$(**1**)) in 0.1 M Bu_4NPF_6–CH_2Cl_2 on 5 μm interdigitated microelectrodes at a sweep rate of 50 mV s^{-1} in each direction from −0.25 V. (b) Cyclic voltammograms of poly($Ru(bpy)_2$(**2**)) sweeping in each direction from −0.6 V. Conditions as in (a).

reduction waves was approximately 2 : 1. Conductivity studies on interdigitated microelectrodes reveal that poly($Ru(bpy)_2$(**1**)) has a maximum conductivity of *ca.* 1×10^{-3} S cm^{-1} at 0.96 V, nearly the same as that of poly(Ru(**1**)$_3$). The self-exchange conductivity due to the reduction of the ruthenium bipyridyl complexes is, however, diminished, being nearly a third of the value of poly(Ru(**1**)$_3$). This difference shows that a cross-linked polymer network facilitates conduction through three dimensions, rather than just by a simple one-dimensional electron hopping mechanism.

The CV of poly($Ru(bpy)_2$(**2**)) also shows differences in comparison to poly(Ru(**2**)$_3$). The reductive region is characterized by a single redox wave at −1.92 V (Fig. 5b). The negative shift of this wave in comparison to the monomer is more substantial than for poly(Ru(**2**)$_3$), which could be caused by the decreased number of electron donating groups on the bipyridine ligands. In the oxidative region the peak areas are again unequal. Integrating the area under the redox waves reveals a 1 : 2 ratio between the reductive and oxidative regions. Conductivity measurements performed on these polymers revealed that the conductivity associated with the $Ru(bpy)_3$ reduction was diminished by an order of magnitude ($\sigma_{max} = 3 \times 10^{-4}$ S cm^{-1} at −1.60 V) compared to that of poly(Ru(**2**)$_3$). This result was expected due to the linear polymer architecture rather than a cross linked polymer. Unfortunately, the polymer has limited stability and the electroactivity diminished with repeated sweeping.

Conclusion

We have synthesized conducting polymer transition metal hybrid materials based on bithienyl-substituted $Ru(bpy)_3$ derivatives. These materials display metal bipyridyl-based and thienyl-based redox processes that exhibit high redox conductivity. Systematic studies of the polymer structure revealed the importance of electronic interactions between the metal complexes through a conjugated polymer backbone. The highest conductivities observed in these systems resulted from a 4,4′- and 4-bithienyl substitution pattern on the bipyridine ligand, indicating that, when the ruthenium complexes are in direct communication through a conjugated organic bridge, self-exchange between ruthenium complexes is more favorable than through space. The ruthenium centers also induce electronic coupling between thienyl groups that ordinarily are not conjugated. This fact is readily apparent from conductivity comparisons between poly(**2**), poly(Ru(**2**)$_3$), and poly($Ru(bpy)_2$(**2**)). We have also shown that cross linking in these polymers is an important contributor to high polymer conductivity and stability. Based upon previous results with related systems,[2,3] further enhancements in the metal-centered redox conductivity will be realized by redox matching the metal centered redox wave with the organic backbone to provide an isoenergetic conduit for electron hopping. Further work on the sensory and catalytic properties of this class of hybrid polymers is ongoing.

Experimental

General procedures

Air- and moisture-sensitive reactions were carried out in oven-dried glassware using standard Schlenk techniques under an inert atmosphere of dry argon. Anhydrous DMF, CH_2Cl_2, and CH_3CN were obtained as sure-seal bottles and used as received. Other reagents were used as received from Aldrich unless otherwise noted. The NMR spectra were recorded with a Bruker AC-250 (^{1}H) or Varian 300 or 500 MHz spectrometer (^{1}H and ^{13}C), UV–Vis absorption spectra on a Hewlett-Packard 8453 diode array spectrophotometer. Electrochemical studies were performed under an air-free dry-box under reduced laboratory lighting using a one compartment cell with either a platinum button or 5 μm interdigitated microelectrode as the working electrode, a platinum coil counter electrode and an isolated silver wire reference electrode. The electrolyte solutions used for all electrochemistry and conductivity measurements were 0.1 M Bu_4NPF_6 in CH_2Cl_2. All electrochemical potentials are reported with reference to the ferrocene–ferrocenium (Fc–Fc^+) redox couple. The thickness of poly(Ru(**1**)$_3$) was determined by profilometry on a Dektak 8000 instrument.

Preparations

4-Nitro-2,2′-bipyridine *N,N′*-dioxide. In a 50 ml round bottom flask, 8 g (79.12 mmol) of KNO_3 and 5 g (26.57 mmol) of 2,2′-bipyridine *N,N′*-dioxide[21] in 13 mL of concentrated H_2SO_4 (95–98%) were heated at 100 °C for 24 h. After cooling to room temperature, the reaction mixture was poured into 500 ml of water and stirred for 2 h. The volume of the aqueous solution was reduced to 150 mL, and neutralized to pH 8. The aqueous solution was thoroughly extracted with $CHCl_3$. Combination and evaporation of the $CHCl_3$ fractions produced the crude mononitro compound which was further purified by chromatography (1% MeOH–$CHCl_3$) to afford 1.01 g (4.33 mmol, 16%) of 4-nitro-2,2′-bipyridine *N,N′*-dioxide (mp 198 °C, decomp.). ^{1}H NMR (500 MHz, DMSO-d_6): δ 8.61 (d, 2 H, J=3.5), 8.56 (d, 2 H, J=7), 8.39 (d, 2 H, J=7), 8.32 (dd, 2 H, J=7 and 3), 7.71 (dd, 2 H, J=8 and 2), 7.58 (td, 2 H, J=7.5 and 2) and 7.46 (t, 2 H, J=7.5 Hz). ^{13}C NMR (125 MHz, DMSO-d_6): δ 143.69, 141.15, 140.8, 140.51, 139.18, 128.75, 127.72, 124.78, 123.20 and 121.33. MS: *m/z* 234 ($[M+H]^+$). HRMS (FAB): found *m/z* 234.0516 ($[M+H]^+$); calc. for $C_{10}H_8N_3O_4$ 234.0515.

4-Bromo-2,2′-bipyridine *N,N′*-dioxide. To a suspension of 1.0 g (4.29 mmol) of 4-nitro-2,2′-bipyridine *N,N′*-dioxide in 15 mL of glacial acetic acid at 60 °C are added 3.0 mL (40.58 mmol) of CH_3COBr. The mixture was refluxed for 2 h and then cooled to room temperature. The solution was poured into 150 g of crushed ice, neutralized with 15% Na_2CO_3, and then dried under vacuum. The resulting solid was suspended in MeOH, stirred for 3 h, and then filtered. The filtrate was evaporated and the resulting solid dried under vacuum to yield 0.74 g (2.77 mmol, 64%) of 4-bromo-2,2′-bipyridine *N,N′*-dioxide as a tan solid (mp >260 °C). ^{1}H NMR (500 MHz, DMSO-d_6): δ 8.35 (d, 1 H, J=6.5), 8.28 (d, 1 H, J=7), 7.99 (d, 1 H, J=2.5), 7.76 (dd, 1 H, J=7 and 3), 7.67 (dd, 1 H, J=7.5 and 2), 7.53 (td, 1 H, J=7.5 and 2) and 7.43 (td, 1 H, J=7.5 and 1). ^{13}C NMR (125 MHz, DMSO-d_6): δ 150.71, 151.0, 149.47, 137.62, 133.29, 127.09, 124.92, 123.3 and 120.85. MS: m/z 267 ($[M+H]^+$). HRMS (FAB): found m/z 266.9773 ($[M+H]^+$); calc. for $C_{10}H_8BrN_2O_2$ 266.9769.

4-Bromo-2,2′-bipyridine. A suspension of 0.4 g (1.50 mmol) of crude 4-bromo-2,2′-bipyridine *N,N′*-dioxide in 12 mL of anhydrous $CHCl_3$ was cooled to −3 °C and 1.4 mL (14.74 mmol) of PBr_3 were added. The mixture was refluxed for 75 min, cooled and poured into ice–water. After phase separation, the organic layer was extracted repeatedly with distilled water, and the aqueous extracts were combined. Neutralization of the aqueous solution with 25% NaOH solution resulted in a white precipitate which was dried under vacuum to afford 0.21 g (0.893 mmol, 60%) of 4-bromo-2,2′-bipyridine. ^{1}H NMR (250 MHz, $CDCl_3$): δ 8.67 (d, 1 H), 8.609 (s, 1 H), 8.46 (d, 1 H), 8.37 (d, 1 H), 7.81 (t, 1 H), 7.46 (d, 1 H) and 7.33 (t, 1 H). MS: m/z 235 ($[M+H]^+$).

4,4′-Bis(5-(2,2′-bithienyl))-2,2′-bipyridine 2. 0.88 g (1.9 mmol) of 5-(tributylstannyl)-2,2′-bithiophene, 0.2 g (0.64 mmol) of 4,4′-dibromo-2,2′-bipyridine, and 0.028 g (0.0399 mmol, 0.05 equivalent) of *trans*-dichlorobis(triphenylphosphine)palladium(II) were combined in 60 mL of DMF and heated at 80–90 °C for 8 h. After removal of the DMF, the resulting solid was chromatographed (silica gel, 2% MeOH–$CHCl_3$) to give compound **2** as a yellow solid in 60% yield. For large scale reactions recrystallization is suggested. ^{1}H NMR (500 MHz, $CDCl_3$): δ 8.70 (d, 2 H, J=5), 8.65 (d, 2 H, J=1.5), 7.59 (d, 2 H, J=4), 7.51 (dd, 2 H, J=5 and 2), 7.28 (td, 4 H, J=5 and 1.5), 7.23 (d, 2 H, J=4) and 7.07 (dd, 2 H, J=5 and 3.5 Hz). The poor solubility of this compound prevented characterization by ^{13}C NMR. MS: m/z 485 ($[M+H]^+$). HRMS (FAB): found m/z 485.0280 ($[M+H]^+$); calc. for $C_{26}H_{17}N_2S_4$ 485.0275. Calc. for $C_{26}H_{16}N_2S_4$: C, 64.46; H, 3.33; N, 5.79. Found: C, 63.13; H, 3.33; N, 5.82%.

4-(5-(2,2′-Bithienyl))-2,2′-bipyridine 3. 0.77 g (1.7 mmol) of 5-(tributylstannyl)-2,2′-bithiophene, 0.2 g (0.85 mmol) of 4-bromo-2,2′-bipyridine, and 0.06 g (0.085 mmol, 0.05 equivalent) of *trans*-dichlorobis(triphenylphosphine)palladium(II) were mixed in 60 mL DMF and heated at 80–90 °C for 6 h under argon. After removal of the DMF, the resulting solid was chromatographed (silica gel, 2% MeOH–CH_2Cl_2) to give 0.15 g (0.468 mmol, 55%) of compound **3** as a yellow solid (mp 112–113 °C). ^{1}H NMR (500 MHz, $CDCl_3$): δ 8.73 (dm, 1 H, J=5), 8.64 (d, 2 H, J=5.5), 8.62 (d, 1 H, J=2), 8.43 (d, 1 H, J=8), 7.85 (td, 1 H, J=7.75 and 2), 7.58 (d, 1 H, J=4), 7.48 (dd, 1 H, J=5.25 and 2), 7.35 (ddd, 1 H, J=7.5 and 4.75 and 3.5), 7.27 (td, 2 H, J=7 and 1), 7.22 (d, 1 H, J=4) and 7.06 (dd, 1 H, J=4.75 and 3.5 Hz). ^{13}C NMR (125 MHz, $CDCl_3$): δ 156.81, 155.86, 149.78, 149.18, 142.02, 139.81, 139.17, 136.95, 136.86, 128.01, 126.36, 125.15, 124.73, 124.34, 123.91, 121.22, 119.39 and 116.78. MS: m/z 321 ($[M+H]^+$). HRMS (FAB): found m/z 321.0516 ($[M+H]^+$); calc. for $C_{18}H_{13}N_2S_2$ 321.0520. Calc. for $C_{18}H_{12}N_2S_2$: C, 67.47; H, 3.77; N, 8.74. Found: C, 67.23; H, 3.54; N, 8.31%.

Tris[4,4′-Bis(5–(2,2′-bithienyl))-2,2′-bipyridine]ruthenium bis(hexafluorophosphate) (Ru(2)$_3$). A 30 mL solution of DMF containing 0.1 g of compound **2** (0.2 mmol) and 0.0143 g (0.068 mmol) $RuCl_3{\cdot}xH_2O$ was refluxed under N_2 for 12 h. After removing the DMF, the residue was dissolved in EtOH and filtered. The filtrate was treated with NH_4PF_6 in EtOH and cooled to 0 °C overnight. The resulting red precipitate was collected and dried under vacuum to afford crude Ru(**2**)$_3$, which was further purified by recrystallization from acetone–MeOH to afford 0.05 g (40%) red solid (mp 248 °C, decomp.). ^{1}H NMR (250 MHz, acetone-d_6): δ 9.25 (s, 6 H), 8.22 (d, 6 H), 8.01 (d, 6 H), 7.78 (dd, 6 H), 7.57 (d, 6 H), 7.49 (d, 6 H), 7.445 (d, 6 H) and 7.15 (t, 6 H). ^{13}C NMR (partially) (125 MHz, acetone-d_6): δ 176.20, 176.17, 176.11, 176.08, 176.07, 176.02, 145.18, 114.37 and 96.13. Calc. for $C_{78}H_{48}F_{12}N_6P_2RuS_{12}{\cdot}8H_2O$: C, 47.08; H, 3.24; N, 4.23. Found: C, 46.67; H, 3.72; N, 4.61%.

Tris[4-(5-(2,2′-bithienyl))-2,2′-bipyridine]ruthenium bis(hexafluorophosphate) (Ru(3)$_3$). This compound was prepared by a procedure similar to that of Ru(**2**)$_3$ except using **3** as the starting material (mp 260 °C, decomp.). ^{1}H NMR (500 MHz, acetone-d_6): δ 9.09 (d, 2 H), 8.27 (m, 2 H), 8.15 (m, 1 H), 8.03 (m, 1 H), 7.76, (s, 1 H), 7.64 (s, 1 H), 7.58 (s, 1 H), 7.48 (s, 1 H), 7.44 (s, 1 H) and 7.16 (s, 1 H). The poor solubility prevented characterization by ^{13}C NMR. Calc. for $C_{54}H_{36}F_{12}N_6P_2RuS_6$: C, 47.96; H, 2.68; N, 6.21. Found: C, 47.42; H, 2.76; N, 6.05%.

Bis(2,2′-bipyridine)[5,5′-bis(5-(2,2′-bithienyl))-2,2′-bipyridine]ruthenium bis(hexafluorophosphate) (Ru(bpy)$_2$(1)). A 50 mL Schlenk flask was charged with 50 mg (0.103 mmol) of compound **1** and 50 mg (0.103 mmol) of *cis*-Ru(bpy)$_2$Cl$_2$ in 25 mL of anhydrous DMF. The red slurry was heated to reflux for 12 h. After cooling to room temperature, the solution was filtered to remove any insoluble material. To the wine red filtrate was added a saturated EtOH solution of NH_4PF_6 to result in a flocculent brick-red precipitate, which was filtered off, washed with EtOH and dried under vacuum to afford 39 mg (0.0328 mmol, 32%) of dark red solid (mp >250 °C). ^{1}H NMR (300 MHz, acetone-d_6): δ 8.93 (d, 1 H, J=8.1), 8.85 (d, 1 H, J=7.8), 8.81 (d, 1 H, J=8.1), 8.44 (dd, 1 H, J=8.7 and 2.1), 8.34–8.32 (m, 2 H), 8.25–8.20 (m, 2 H), 8.00 (d, 1 H, J=1.8), 7.72 (ddd, 1 H, J=7.65, 5.7 and 1.5), 7.61 (ddd, 1 H, J=7.58, 5.7, and 1.2), 7.54 (dd, 1 H, J=4.95 and 1.2), 7.41 (d, 1 H, J=3.9), 7.32 (dd, 1 H, J=3.75 and 1.2), 7.30 (d, 1 H, J=3.9), 7.12 (dd, 1 H, J=5.25 and 3.9 Hz). The poor solubility prevented characterization by ^{13}C NMR. MS: m/z 898 ($[M-2PF_6+H]^+$). HRMS (FAB): found m/z 899.0674 ($[M\text{-}2PF_6+H]^+$); calc. for $C_{46}H_{33}N_6RuS_4$ 899.0693. Calc. for $C_{46}H_{32}F_{12}N_6P_2RuS_4$: C, 46.50; H, 2.71; N, 7.07. Found: C, 46.53; H, 2.69; N, 7.12%.

Bis(2,2′-bipyridine)[4,4′-bis(5-(2,2′-bithienyl))-2,2′-bipyridine]ruthenium bis(hexafluorophosphate) (Ru(bpy)$_2$(2)). A 50 mL Schlenk flask was charged with 50 mg (0.103 mmol) of compound **2** and 50 mg (0.103 mmol) of *cis*-Ru(bpy)$_2$Cl$_2$. 25 mL of degassed EtOH were added and the dark red slurry was refluxed for 12 h. After cooling to room temperature, the solution was filtered to remove any insoluble material. To the wine red filtrate was added a saturated EtOH solution of NH_4PF_6 to result in a flocculent brick-red precipitate, which was filtered off, washed with EtOH and dried under vacuum to afford 44 mg (0.037 mmol, 36%) of brick red solid (mp >250 °C). ^{1}H NMR (500 MHz, acetone-d_6): δ 9.20 (d, 2 H, J=2), 8.86 (d, 2 H, J=4), 8.27–8.25 (m, 2 H), 8.24 (dd, 2 H, J=3.75 and 1.5), 8.22 (dd, 2 H, J=4 and 1.5), 8.09

(dm, 2 H, $J=2$), 8.01 (s, 2 H), 8.00 (d, 2 H, $J=4$), 7.74 (dd, 2 H, $J=6.25$ and 2.5), 7.62 (dtd, 4 H, $J=7.5$, 5.75 and 1), 7.58 (dd, 2 H, $J=5$ and 1), 7.49 (d, 2 H, $J=4$), 7.46 (dd, 2 H, $J=3.75$ and 1.5) and 7.17 (dd, 2 H, $J=5.25$ and 4 Hz). The poor solubility prevented characterization by ^{13}C NMR. MS: m/z 897 ($[M-2PF_6+H]^+$). HRMS (FAB): found m/z 899.0682 ($[M\text{-}2PF_6+H]^+$); calc. for $C_{46}H_{33}N_6RuS_4$ 899.0693. Calc. for $C_{46}H_{32}F_{12}N_6P_2RuS_4$: C, 46.50; H, 2.71; N, 7.07. Found: C, 46.25; H, 2.62; N, 6.74%.

Acknowledgements

We acknowledge funding from the Office of Naval Research and Union Carbide Corporation.

References

1 S. S. Zhu and T. M. Swager, *Adv. Mater.*, 1996, **8**, 497.
2 S. S. Zhu, P. J. Carroll and T. M. Swager, *J. Am. Chem. Soc.*, 1996, **118**, 8713; S. S. Zhu and T. M. Swager, *J. Am. Chem. Soc.*, 1997, **119**, 12568.
3 R. P. Kingsborough and T. M. Swager, *Adv. Mater.*, 1998, **10**, 1100.
4 P. G. Pickup and C. G. Cameron, *Chem. Commun.*, 1997, 303.
5 G. Zotti, S. Zecchin, G. Schiavon, A. Berlin, G. Pagani and A. Canavesi, *Chem. Mater.*, 1995, **7**, 2309.
6 P. L. Vidal, M. Billon, B. Divisia-Blohorn, G. Bidan, J. M. Kern and J. P. Sauvage, *Chem. Commun.*, 1998, 629.
7 G. Bidan, B. Divisia-Blohorn, M. Lapkowski, J. M. Kern and J. P. Sauvage, *J. Am. Chem. Soc.*, 1992, **114**, 5986; G. Bidan, B. Divisia-Blohorn, M. Billon, J. M. Kern and J. P. Sauvage, *J. Electroanal. Chem. Interfacial Electrochem.*, 1993, **360**, 189; J. M. Kern, J. P. Sauvage, G. Bidan, M. Billon and B. Divisia-Blohorn, *Adv. Mater.*, 1996, **8**, 580.
8 T. Yamamoto, Y. Yoneda and T. Maruyama, *J. Chem. Soc., Chem. Commun.*, 1992, 1652; T. Yamamoto, T. Maruyama, Z. Zhou, T. Ito, T. Fukuda, Y. Yoneda, F. Begum, T. Ikeda, S. Sasaki, H. Takezoe, A. Fukuda and K. Kubota, *J. Am. Chem. Soc.*, 1994, **116**, 4832.
9 A. Deronzier and J. C. Moutet, *Acc. Chem. Res.*, 1989, **22**, 249.
10 H. D. Abruña, in *Electroresponsive Molecular and Polymeric Systems*, ed. T. A. Skotheim, Marcel Dekker, New York, 1988, ch. 3 and ref. therein.
11 Z. Peng and L. Yu, *J. Am. Chem. Soc.*, 1996, **118**, 3777.
12 (*a*) C. D. Ellis, W. R. Murphy, Jr. and T. J. Meyer, *J. Am. Chem. Soc.*, 1981, **103**, 7480; (*b*) H. D. Abruña, P. Denisevich, M. Umaña, T. J. Meyer and R. W. Murray, *J. Am. Chem. Soc.*, 1981, **103**, 1; (*c*) C. D. Ellis, L. D. Margerum, R. W. Murray and T. J. Meyer, *Inorg. Chem.*, 1983, **22**, 1283; (*d*) P. G. Pickup, W. Kutner, C. R. Leidner and R. W. Murray, *J. Am. Chem. Soc.*, 1984, **106**, 1991; (*e*) C. E. D. Chidsey and R. W. Murray, *J. Phys. Chem.*, 1986, **90**, 1479; (*f*) P. Denisevich, K. W. Willman and R. W. Murray, *J. Am. Chem. Soc.*, 1981, **103**, 4727.
13 V. Grosshenny, A. Harriman, J. P. Gisselbrecht and R. Ziesel, *J. Am. Chem. Soc.*, 1996, **118**, 10315.
14 J. A. Moss, R. Argazzi, C. A. Bignozzi and T. J. Meyer, *Inorg. Chem.*, 1997, **36**, 762.
15 S. C. Rasmussen, D. W. Thompson, V. Singh and J. D. Peterson, *Inorg. Chem.*, 1996, **35**, 3449.
16 E. W. Neuse, *J. Macromol. Sci., Chem.*, 1981, A16, 3 and refs. therein.
17 H. W. Segawa, F.-P. Wu, N. Nakayama, H. Maruyama, S. Sagisaka, N. Higuchi, M. Fujitsuka and T. Shimidzu, *Synth. Met.*, 1995, **71**, 2151; J. L. Reddinger and J. R. Reynolds, *Macromolecules*, 1997, **30**, 673; *Synth. Met.*, 1997, **84**, 225; *Chem. Mater.*, 1998, **10**, 3; 1236.
18 R. P. Kingsborough and T. M. Swager, *Prog. Inorg. Chem.*, 1999, **48**, 123.
19 C. P. Whittle, *J. Heterocycl. Chem.*, 1977, **14**, 191.
20 G. Maerker and F. H. Case, *J. Org. Chem.*, 1958, **80**, 2745.
21 S. Anderson, E. C. Constable, K. R. Seddon, J. E. Turp, J. E. Baggot and M. J. Pilling, *J. Chem. Soc., Dalton Trans.*, 1985, 2247.
22 C. M. Elliot and E. J. Hershehart, *J. Am. Chem. Soc.*, 1982, **104**, 7519.
23 R. J. Watts and G. A. Crosby, *J. Am. Chem. Soc.*, 1981, **93**, 3184; G. D. Hager, R. J. Watts and G. A. Crosby, *J. Am. Chem. Soc.*, 1975, **97**, 7037.
24 K. Kalyanasundaram, *Coord. Chem. Rev.*, 1982, **46**, 159 and refs. therein.
25 H. B. Ross, M. Boldaji, D. P. Rillema, C. B. Blanton and R. P. White, *Inorg. Chem.*, 1989, **28**, 1013.
26 A. Juris, S. Campagna, V. Balzani and G. Gremaud, *Inorg. Chem.*, 1988, **27**, 3652.
27 D. P. Rillema, G. Allen, T. J. Meyer and D. Conrad, *Inorg. Chem.*, 1983, **22**, 1617.
28 Y. Oshawa, K. W. Hanck and M. K. DeArmond, *J. Electroanal. Chem. Interfacial Electrochem.*, 1984, **175**, 229.
29 D. E. Morris, Y. Oshawa, D. P. Segers, M. K. DeArmond and K. W. Hanck, *Inorg. Chem.*, 1984, **23**, 3010.
30 T. J. Meyer, *Acc. Chem. Res.*, 1978, **11**, 94 and refs. therein; P. Mabrouk and M. S. Wrighton, *Inorg. Chem.*, 1986, **25**, 526.
31 (*a*) E. W. Paul, A. J. Ricco and M. S. Wrighton, *J. Phys. Chem.*, 1985, **89**, 1441; (*b*) J. W. Thackeray, J. W. White and M. S. Wrighton, *J. Phys. Chem.*, 1985, **89**, 5133; (*c*) G. P. Kittlesen, H. S. White and M. S. Wrighton, *J. Am. Chem. Soc.*, 1984, **106**, 7389; (*d*) D. Ofer, R. M. Crooks and M. S. Wrighton, *J. Am. Chem. Soc.*, 1990, **112**, 7869.
32 G. Zotti, G. Schiavon and S. Zecchin, *Synth. Met.*, 1995, **72**, 275; R. M. Crooks, O. M. Chyan and M. S. Wrighton, *Chem. Mater.*, 1989, **1**, 2; R. Borjas and D. A. Buttry, *Chem. Mater.*, 1991, **3**, 872.

Paper 9/03193F